

# NO EVIDENCE OF CIRCUMSTELLAR GAS SURROUNDING TYPE IA SUPERNOVA SN 2017cbv

RAPHAEL FERRETTI,<sup>1</sup> RAHMAN AMANULLAH,<sup>1</sup> MATTIA BULLA,<sup>1</sup> ARIEL GOOBAR,<sup>1</sup> JOEL JOHANSSON,<sup>2,3</sup> AND  
PETER LUNDQVIST<sup>4</sup>

<sup>1</sup>*Oskar Klein Centre, Department of Physics, Stockholm University, Albanova, SE 106 91 Stockholm, Sweden*

<sup>2</sup>*Ben-Ziyo Center for Astrophysics, Weizmann Institute of Science, 76100 Rehovot, Israel*

<sup>3</sup>*Department of Physics and Astronomy, Division of Astronomy and Space Physics, Uppsala University, Box 516, SE 751 20 Uppsala, Sweden*

<sup>4</sup>*Oskar Klein Centre, Department of Astronomy, Stockholm University, Albanova, SE 106 91 Stockholm, Sweden*

(Received; Revised; Accepted)

Submitted to ApJL

## ABSTRACT

Nearby type Ia supernovae (SNe Ia), such as SN 2017cbv, are useful events to address the question of what the elusive progenitor systems of the explosions are. [Hosseinzadeh et al. \(2017a\)](#) suggested that the early blue excess of the lightcurve of SN 2017cbv could be due to the supernova ejecta interacting with a nondegenerate companion star. Some SN Ia progenitor models suggest the existence of circumstellar (CS) environments in which strong outflows create low density cavities of different radii. Matter deposited at the edges of the cavities, should be at distances at which photoionisation due to early ultraviolet (UV) radiation of SNe Ia causes detectable changes to the observable Na I D and Ca II H&K absorption lines. To study possible narrow absorption lines from such material, we obtained a time-series of high-resolution spectra of SN 2017cbv at phases between  $-14.8$  and  $+83$  days with respect to  $B$ -band maximum, covering the time at which photoionisation is predicted to occur. Both narrow Na I D and Ca II H&K are detected in all spectra, with no measurable changes between the epochs. We use photoionisation models to rule out the presence of Na I and Ca II gas clouds along the line-of-sight of SN 2017cbv between  $\sim 8 \times 10^{16}$ – $2 \times 10^{19}$  cm and Ca II within  $\sim 10^{15}$ – $10^{17}$  cm, respectively. Assuming typical abundances, the mass of a homogenous spherical CS gas shell with radius  $R$  must be limited to  $M_{\text{H I}}^{\text{CSM}} < 3 \times 10^{-4} \times (R/10^{17}[\text{cm}])^2 M_{\odot}$ . The bounds point to progenitor models that deposit little gas in their CS environment.

*Keywords:* supernovae: individual (SN 2017cbv)

## 1. INTRODUCTION

Type Ia supernovae (SNe Ia) are of great importance to modern cosmology, because they are standardisable candles (see e.g. [Goobar & Leibundgut 2011](#), for a review). Although thousands of SNe Ia have been observed, the physics of the progenitor system leading to the explosions is not fully understood. There are two prevalent progenitor models for SNe Ia, both of which have some observational support. The models involve the thermonuclear explosion of a carbon-oxygen (C/O) white dwarf (WD) in a binary system with another star, which it merges with or accretes mass from. If the companion star is another WD, the system is referred to as a double degenerate (DD, [Iben & Tutukov 1984](#); [Webbink 1984](#)), and if it is a main sequence or giant star, a single degenerate progenitor (SD, [Whelan & Iben 1973](#)). More complicated systems, such as common envelope (or symbiotic) binaries ([Dilday et al. 2012](#)), and colliding WDs have also been proposed ([Dong et al. 2015](#)).

The circumstellar (CS) environment of SNe Ia should hold clues to the progenitor systems. SD progenitors for instance are believed to have strong outflows, which excavate low density cavities into the surrounding interstellar medium (ISM) and deposit matter at the edges ([Badenes et al. 2007](#)). Similarly, DD Helium+C/O binary systems should create cavities with smaller radii ([Shen et al. 2013](#)). On much smaller scales, tidal effects in DD progenitors can deposit matter into the CS medium ([Raskin & Kasen 2013](#)).

Strong upper limits on outflowing matter have been set with radio ([Chomiuk et al. 2016](#); [Kundu et al. 2017](#)) and X-ray ([Margutti et al. 2014](#)) observations of individual SNe Ia. Furthermore, the lack of thermal emission in mid- and far-infrared wavelengths, has set strong limits on the presence of CS dust ([Johansson et al. 2013, 2017](#)). Nevertheless, observations such as predominately blueshifted profiles of narrow Na I D absorption lines point to outflowing material along the lines-of-sight (LOS) ([Sternberg et al. 2011](#); [Maguire et al. 2013](#)). However, the blueshifted profiles and frequently observed large Na I column densities ([Phillips et al. 2013](#)) could also be explained by desorption from ISM dust grains, when they are exposed to the radiation of SNe Ia ([Soker 2014](#)).

Along with a recent method, which follows variable reddening of SNe Ia ([Bulla et al. 2018](#)), variations in narrow absorption line profiles can be used to locate gas close to SNe Ia. Before maximum brightness, photoionisation should lead to a decrease of characteristic absorption lines ([Borkowski et al. 2009](#)). At later phases recombination of the same gas could lead to the increase in the same absorption lines. Variations due to pho-

toionisation can be used to determine the distance of the gas from a supernova. However, geometric effects ([Patat et al. 2010](#)) and changing levels of foreground light ([Maeda et al. 2016](#)) can also lead to similar variations.

A small number of SNe Ia with variable absorption lines have been observed to date:

- SN 2006X ([Patat et al. 2007](#)) showed a changing Na I D profile at late times, which could point to recombination or geometric effects ([Chugai 2008](#)).
- SN 2007le ([Simon et al. 2009](#)) showed an increasing Na I D component.
- SN 2011fe ([Patat et al. 2013](#)) showed slight variations, consistent with geometric effects.
- PTF11kx ([Dilday et al. 2012](#)), a peculiar supernova which showed many variable absorption features and is believed to have had a symbiotic progenitor.
- SN 2013gh ([Ferretti et al. 2016](#)) had a varying Na I D component consistent with photoionisation.
- SN 2014J ([Graham et al. 2015](#)) showed a varying K I line while Na I D remained unchanged, which is consistent with photoionisation, although [Maeda et al. \(2016\)](#) argue that the gas is unlikely to have been CS matter.

A larger sample of 14 SNe Ia with multi-epoch high-resolution spectra ([Sternberg et al. 2014](#)), did not reveal further examples of varying absorption lines. However, almost all existing time-series are taken at too late phases to probe for photoionisation of CS gas (see [Ferretti et al. 2016](#)).

Because of its low redshift, early discovery and a LOS seemingly clear of an ISM, the recently discovered SN 2017cbv ([Hosseinizadeh et al. 2017a](#)) presents a good opportunity to search for photoionisation of CS gases. Below we present the high-resolution spectra we obtained (Section 2), in which we identify narrow Na I D and Ca II H&K absorption features and search for variations in them (Section 3). Using a simple photoionisation model, we then set limits on the presence of CS gases (Section 4). Finally, we compare our observations to the findings of [Hosseinizadeh et al. \(2017a\)](#) and conclude (Section 5 & 6).

## 2. OBSERVATIONS

SN 2017cbv was discovered on March 10 UT (MJD 57822.14) by the Distance Less Than 40 Mpc (DLT40)

MJD	UT Date	Exp. time (s)	Set-up	Epoch (days)	$R$ ( $\lambda/\delta\lambda$ )	$S/N^\dagger$	H <sub>2</sub> O column (mm)
57826.3	Mar. 14.3	1800	1.0" DIC1 390+580	-14.8	62,000	110	$13.6 \pm 0.3$
57831.2	Mar. 19.2	$2 \times 1700$	0.8" DIC1 390+580	-9.9	66,000	150	$6.3 \pm 0.1$
57846.1	Apr. 03.1	$2 \times 2000$	0.8" DIC1 390+580	5.0	52,000	210	$1.4 \pm 0.1$
57923.2	Jun. 19.2	$2 \times 1700$	0.8" DIC1 390+580	82.1	56,000	}110	$1.2 \pm 0.2$
57924.0	Jun. 20.0	$2 \times 1700$	0.8" DIC1 390+580	82.9	63,000		$2.1 \pm 0.2$

<sup>†</sup>around 5900 Å

**Table 1.** The obtained UVES spectra. Epochs are with respect to the  $B$ -band maximum on MJD 57841.1 (Hossein-zadeh et al. 2017a). Resolutions are inferred from the full-width-half-maxima of several telluric lines and the H<sub>2</sub>O columns were computed with Molecfit.

supernova survey (Tartaglia et al. 2017) and subsequently classified as a young SN Ia (Hossein-zadeh et al. 2017b). The supernova is located in the outskirts of NGC 5643 at  $z = 0.003999(7)$  (Koribalski et al. 2004), at  $\alpha = 14^h 32^m 34.42^s$ ,  $\delta = -44^\circ 08' 02.8''$  (J2000), a LOS with galactic extinction  $E(B - V)_{MW} = 0.15$  mag (Schlafly & Finkbeiner 2011). Lightcurve analysis by Hossein-zadeh et al. (2017a) determined that SN 2017cbv peaked at MJD 57841.07 in  $B$ -band with  $\Delta m_{15}(B) = 1.06$  mag.

Because SN 2017cbv was a good candidate to search for CS gas, we triggered our ESO TOOs 098.A-0783(A) and 098.A-0783(B) (P.I. Amanullah) to obtain spectra with the Ultraviolet and Visual Echelle Spectrograph (UVES; Dekker et al. 2000) on UT2 at the Very Large Telescope (VLT). We reduced the spectra using the REFLEX (ESOREX) reduction pipeline provided by ESO (Modigliani et al. 2010) and used the telluric line correction software Molecfit (Smette et al. 2015; Kausch et al. 2015) where necessary. The obtained spectra are summarised in Table 1.

The first UVES spectrum was taken on MJD 57826.3, 4.2 days after discovery, at an epoch of  $-14.8$  days before  $B$ -band maximum. Two follow-up spectra were obtained bracketing maximum light to cover the time frame at which changes due to photoionisation could be expected. Finally, two late spectra were taken on back-to-back nights to cover phases during which late-time absorption line variations have been observed in the past (e.g. SN 2006X, Patat et al. 2007). In the following, the two last spectra are treated as one epoch, since SNe Ia only evolve slowly at late phases and an improved signal-to-noise ratio ( $S/N$ ) is achieved by coadding them.

### 3. NARROW ABSORPTION FEATURES

We searched all spectra for narrow absorption features in the rest frame of NGC 5643. While Ca II H&K lines were immediately apparent in all spectra, Na I D ab-

sorption was only revealed after applying telluric line corrections. We searched for, but did not detect CH and CH+ or any diffuse interstellar bands (DIBs) such as those identified in Sollerman et al. (2005). The frequently studied DIBs at  $\lambda\lambda$  5780 and 5797 fall in between the spectral arms of the UVES spectra and K I lies outside the range of the instrument with the chosen set up.

Around  $z = 0.004$ , many telluric lines can make the identification of Na I D difficult. In fact the telluric features in the first two epochs are more prominent than Na I D. In Table 1 the H<sub>2</sub>O column determined from telluric line fitting is shown for reference. The Na I D features could be identified because,

- several features remained after telluric line correction at the redshift of NGC 5643,
- they appeared as doublets with the separation and line ratios characteristic of Na I D,
- they did not shift with the telluric lines between epochs,
- and they appeared to have the same rest frame velocity as the deepest features of Ca II H&K.

The detected absorption lines are plotted in Figure 1 after normalising the continua and correcting for telluric features.

We visually compared the profiles of each epoch for differences. In the first epoch a small peak appears in next to the most redshifted feature in Na I D2 (labeled VIII in Figure 1). Notably, there is no feature at the corresponding wavelength in Na I D1 and several comparable outliers can be identified in the continuum of this spectrum. For this reason we ignore the peak in the further analysis. No other significant differences could be visually identified between the epochs.

To search for absorption line variations, we measured the pixel-for-pixel equivalent widths ( $W$ ) of each epoch.

Where possible, we measured  $W$  of individual features or, if the lines are blended, across groups of features. In neither case significant trends could be identified. The average total values measured are  $W_{\text{Na I D1}} = 13.9 \pm 1.4$ ,  $W_{\text{Na I D2}} = 31.2 \pm 1.3$ ,  $W_{\text{Ca II H}} = 69.3 \pm 2.5$  and  $W_{\text{Ca II K}} = 123.5 \pm 2.5$  mÅ.

We further fit Voigt profiles to the features using VP-FIT<sup>1</sup>, whereby we fit the profiles of each doublet of the same absorber simultaneously (Na I D1 with D2 and Ca II H with K). To establish the best over all profile, we initially fit all epochs simultaneously. The Ca II H&K profiles can be fit well by eight individual components, while four of those match the profile of Na I D. In Table 2, the Voigt profile parameters, redshift ( $z$ ), column density ( $N_X$ ), and Doppler widths ( $b_X$ ), of the simultaneous fits are presented, whereby the features are labeled the same way as in Figure 1.

The most prominent features IV–VI and VIII have close enough redshifts in both Na I D and Ca II H&K to correspond to the same gas clouds along the LOS to SN 2017cbv. Interestingly,  $b_{\text{Ca II}}$  of these features appear to be significantly larger than  $b_{\text{Na I}}$ . This suggests either that there are more unresolved features in Ca II H&K, or Ca II is depleted in the colder regions of these gas clouds. The ratios ( $N_{\text{Ca II}}/N_{\text{Na I}}$ ) of these features are also shown in Table 2.

To search for time dependence, we fit the Voigt profiles to each epoch individually. The profiles are plotted in red over the spectra in Figure 1. We studied  $N_X$  and  $b_X$  of each feature without finding any significant trends. In Figure 2 it can be seen that  $N_X$  of the most prominent features are consistent with the values determined from the simultaneous fits of all epochs.

#### 4. PHOTOIONISATION

We use a photoionisation model described in Borkowski et al. (2009), in which we assume a homogenous thin shell of CS gas that is optically thin to ionising photons. The fraction of such a gas  $X$  in a shell of radius  $R$  that is ionised at a given time is

$$I_X(t; R) = \frac{D^2}{R^2} \int_0^{\lambda_I} \alpha_X(\lambda) \frac{f_\lambda(\lambda, t)}{hc} \lambda d\lambda, \quad (1)$$

where  $f_\lambda(\lambda, t)$  is the spectral energy distribution (SED) of a supernova at a distance  $D$  from the observer,  $\alpha_X(\lambda)$  is the wavelength dependent ionisation cross-section<sup>2</sup> (Huebner & Mukherjee 2015) and  $\lambda_I$  the ionisation energy of the gas. The column density  $N_X(t)$  is then de-

fined by

$$\frac{dN_X(t)}{dt} = -N_X(t)I_X(t; R), \quad (2)$$

which implies that

$$N_X(t'; R, N_0) = N_0 \exp \left\{ - \int_{t_0}^{t'} I_X(t; R) dt \right\}. \quad (3)$$

We use the SED from Amanullah et al. (2015) based on SN 2011fe, since this supernova has the best temporal coverage of high S/N ultraviolet (UV) spectra.  $N_X(t)$  then depends on two free parameters, the initial column density  $N_0$  and  $R$ .

In the absence of absorption line variations, the model can be used to set limits on  $R$  and  $N_0$ . For a given set of observations, one can define a range  $R_X^{\text{excl.}}$ , within which any gas would be ionised. Thereby  $R_X^{\text{inner}}$  defines the radius at which all gas is ionised before the first spectrum is obtained and  $R_X^{\text{outer}}$  is the radius beyond which the ionising flux is negligible. To obtain a strong inner radius limit, the first spectrum must be obtained as early as possible.

The spectral coverage of SN 2017cbv implies that  $R_{\text{Na I}}^{\text{excl.}} \approx 5 \times 10^{16} - 2 \times 10^{19}$  cm and  $R_{\text{Ca II}}^{\text{excl.}} \approx 6 \times 10^{14} - 10^{17}$  cm. In Figure 3 the fractional ionisation curves at  $R_{\text{Na I}}^{\text{inner}}$  and  $R_{\text{Ca II}}^{\text{inner}}$  are shown. Since the ultraviolet (UV) flux of SNe Ia can vary considerably between supernovae, we consider a  $\pm 1$  mag (factor 2.5) range in UV flux. If the SED underestimates the UV flux of SN 2017cbv by this factor,  $R_{\text{Na I}}^{\text{inner}} \approx 8 \times 10^{16}$  cm and  $R_{\text{Ca II}}^{\text{inner}} \approx 10^{15}$  cm.

One can furthermore define  $N_X^{\text{upper}}$ , the highest column density a gas cloud within the excluded radius range can have to not be detected. In the cases of Na I and Ca II gas, one can require that an absorption feature must be identifiable in both profiles of the Na I D and Ca II H&K. This implies it must be detectable in Na I D1 and Ca II H, which have the weaker oscillator strengths of their respective doublets.

Assuming a feature with a Gaussian profile and a full-width-half-maximum of 0.1 Å, the column density would need to be more than  $\log_{10}\{N_{\text{Na I}}^{\text{upper}} [cm^{-2}]\} = 10.4$  for a line to be identifiable above the noise in Na I D1. Notably, feature IV has a lower column density than this limit and is not detected in Na I D1 above the noise of the first epoch. Only in the later spectra, with higher S/N and lower water column, feature IV can be identified. Using the same criterion, a column density greater than  $\log_{10}\{N_{\text{Ca II}}^{\text{upper}} [cm^{-2}]\} = 10.7$  is necessary to identify a feature in Ca II H in the first epoch.

One can further determine an upper bound on the enclosed mass of CS gas from the upper column density

<sup>1</sup> <http://www.ast.cam.ac.uk/~rfc/vpfit.html>

<sup>2</sup> Obtained via [phidrates.space.swri.edu](http://phidrates.space.swri.edu)

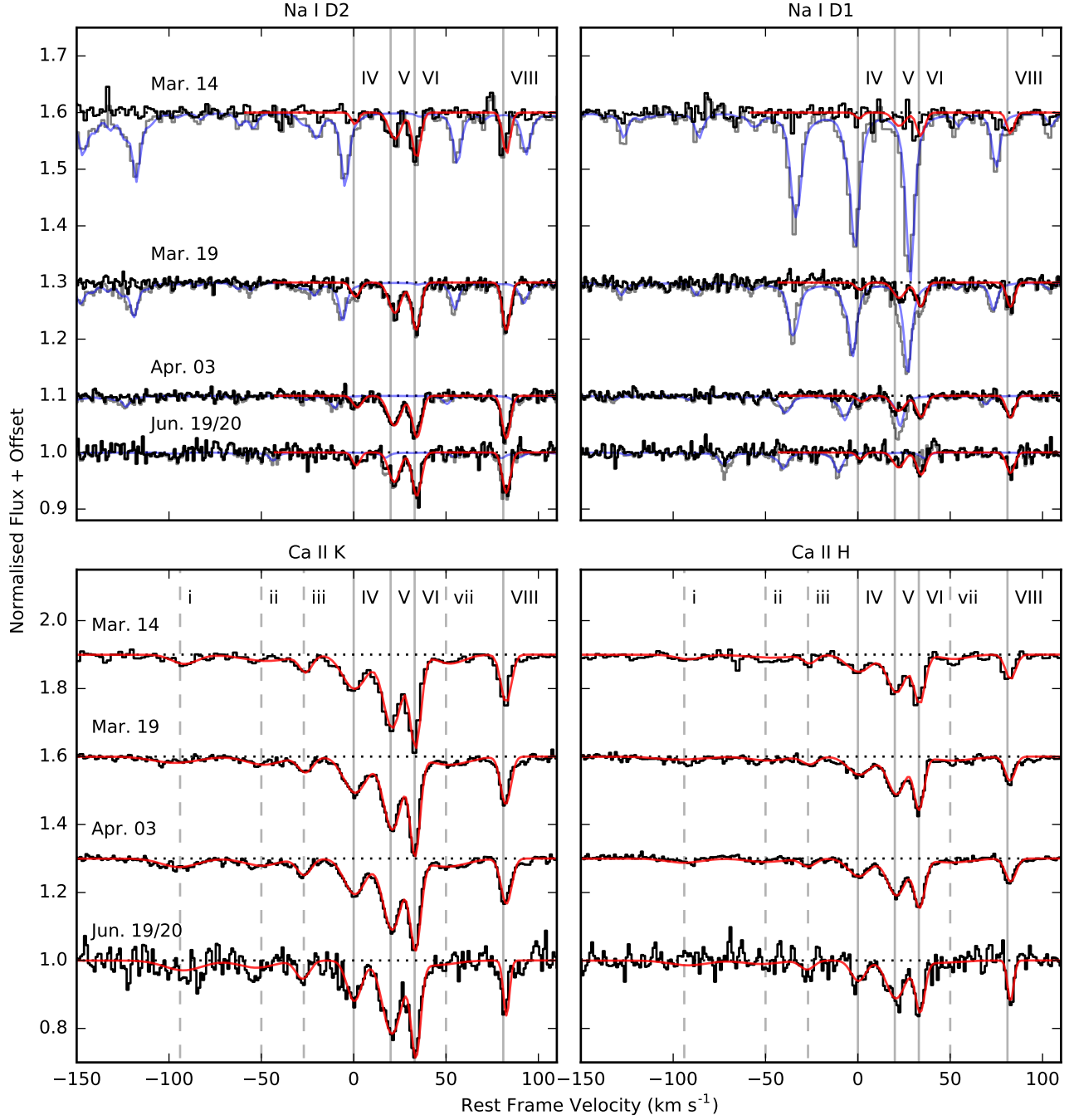


**Figure 1.** The detected Na I D and Ca II H&K features in velocity space of the host galaxy rest frame at  $z = 0.004$ . For clarity, the spectra, which are shown in black, have been normalised, offset and, in the case of Na I D, telluric line corrected. The uncorrected spectra are shown in grey along with the telluric line model in light blue. The fitted Voigt profiles are plotted in red and vertical lines indicate individual line components. Features present in both Na I D and Ca II H&K are marked with solid grey lines and labeled with capital Roman numerals, while features only detected in Ca II H&K with dashed grey lines and lower case Roman numerals.

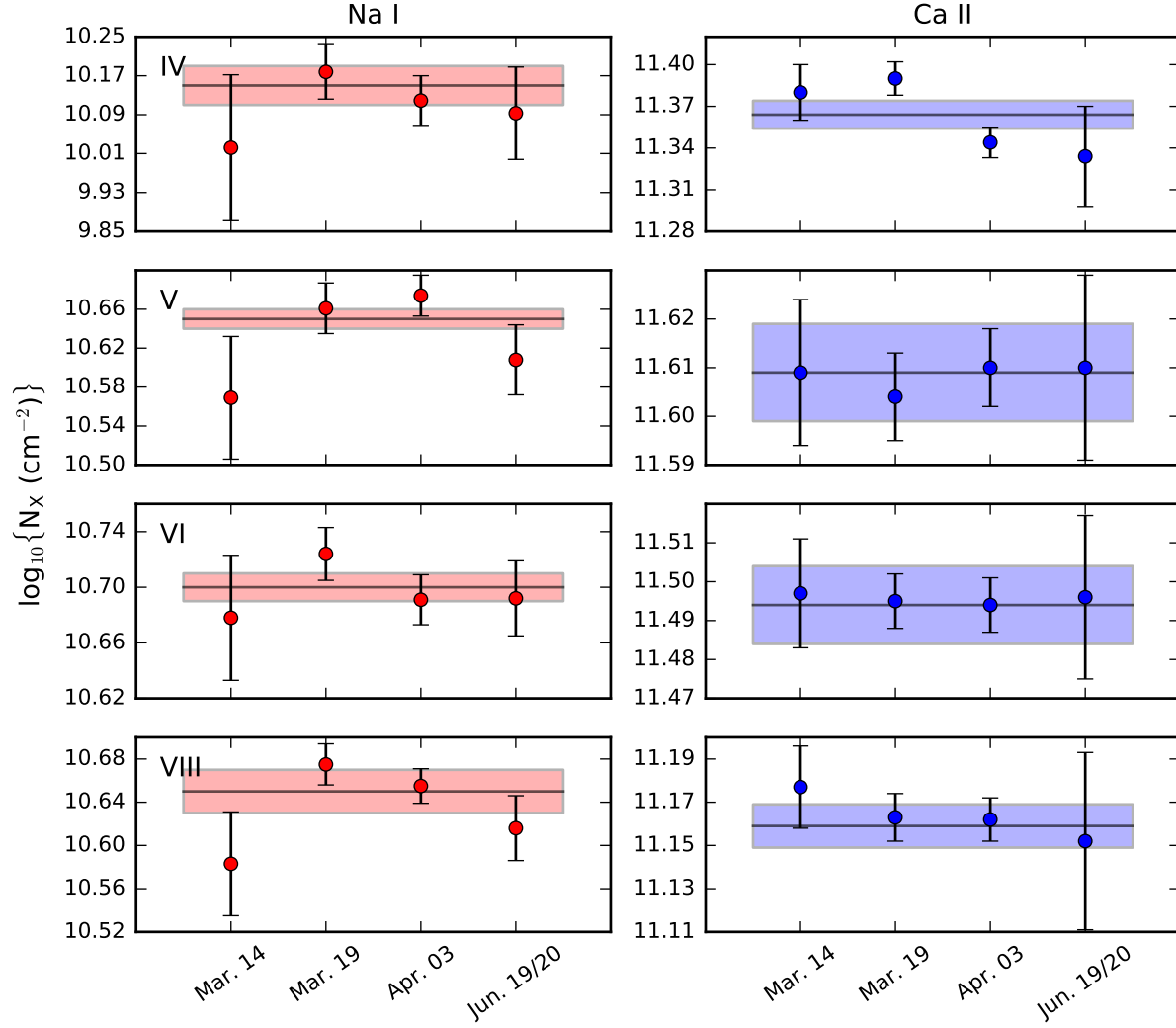


**Figure 2.** Column densities of the four most prominent absorption features IV, V, VI and VIII inferred from the Voigt profile fits. The data points are computed from each epoch individually with  $1\sigma$  error-bars, while the horizontal lines are determined by the simultaneous fit of all epochs with a  $1\sigma$  band.

Feature	$v^\dagger$ (km s <sup>-1</sup> )	$z_{\text{Na I}}$	$\log_{10}\{N_{\text{Na I}}\}$ (cm <sup>-2</sup> )	$b_{\text{Na I}}$ (km s <sup>-1</sup> )	$z_{\text{Ca II}}$	$\log_{10}\{N_{\text{Ca II}}\}$ (cm <sup>-2</sup> )	$b_{\text{Ca II}}$ (km s <sup>-1</sup> )	$N_{\text{Ca II}}/N_{\text{Na I}}$
i	-94	–	–	–	0.003684(2)	$10.92 \pm 0.03$	$14.1 \pm 1.0$	–
ii	-50	–	–	–	0.003834(3)	$10.85 \pm 0.03$	$12.3 \pm 1.2$	–
iii	-27	–	–	–	0.003911(1)	$10.83 \pm 0.02$	$4.6 \pm 0.5$	–
IV	1	0.004005(1)	$10.15 \pm 0.03$	$1.7 \pm 0.7$	0.004002(1)	$11.37 \pm 0.01$	$7.8 \pm 0.2$	17.4
V	21	0.004074(1)	$10.66 \pm 0.01$	$3.5 \pm 0.3$	0.004070(1)	$11.60 \pm 0.01$	$5.9 \pm 0.1$	8.9
VI	33	0.004114(1)	$10.72 \pm 0.01$	$1.5 \pm 0.3$	0.004112(1)	$11.50 \pm 0.01$	$2.4 \pm 0.1$	6.2
vii	50	–	–	–	0.004168(4)	$10.98 \pm 0.04$	$15.1 \pm 1.5$	–
VIII	82	0.004277(1)	$10.67 \pm 0.02$	$0.7 \pm 0.4$	0.004276(1)	$11.16 \pm 0.01$	$2.3 \pm 0.2$	3.2

<sup>†</sup> inferred from  $z_{\text{Ca II}}$  with respect to  $z = 0.003999$

**Table 2.** Redshifts  $z_X$ , Column densities  $N_X$  and Doppler widths of  $b_X$  of the fitted Voigt profile components. The values are the average parameters obtained from fitting the profiles of each spectrum. Features are labeled the same way as in Figure 1, where capital roman numerals correspond to features detected in both Na I D and Ca II H&K, while the lower case roman numerals correspond to features only detected in Ca II H&K.

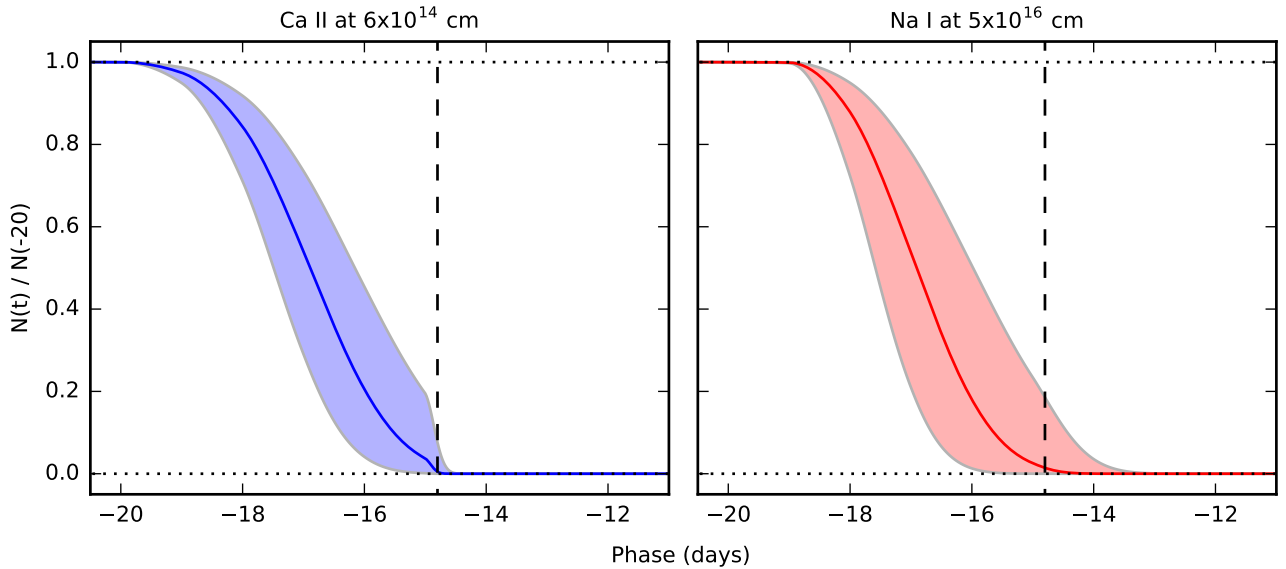


**Figure 3.** Na I and Ca II ionisation curves at the inner exclusion limit. Any gas clouds closer to a SN Ia than those shown are ionised before an epoch of  $-14.8$  days. The bands show the changes in the ionisation fraction if the UV flux of the SN varies by  $\pm 1$  mag (factor 2.5).

limits. Assuming a homogenous shell of gas with a radius  $R$ ,  $M_{\text{Na I}}^{\text{CSM}} < 6 \times 10^{-11} \times (R/10^{17}[\text{cm}])^2 M_{\odot}$  and  $M_{\text{Ca II}}^{\text{CSM}} < 2 \times 10^{-10} \times (R/10^{17}[\text{cm}])^2 M_{\odot}$ , where the values are scaled to  $R = 10^{17}$  cm. For typical abundances of  $N_{\text{Na I}}/N_{\text{H I}} \sim 10^{-8}$  (Wakker & Mathis 2000), this suggests an H I mass of  $M_{\text{H I}}^{\text{CSM}} < 3 \times 10^{-4} \times (R/10^{17}[\text{cm}])^2 M_{\odot}$ . If the gas has been swept up from the ISM surrounding the progenitor, the H I volume density must have been  $< 10^2 \times ((10^{17}[\text{cm}])/R) \text{ cm}^{-3}$ .

After photoionisation, gas is expected to recombine, whereby the recombination rate is dependent on the

temperature and electron density of the gas cloud. To describe recombination on the time scale of the variations observed in SNe 2006X and 2007le, high electron densities must be assumed (e.g.  $10^7 \text{ cm}^{-3}$ , Simon et al. 2009). This has led to alternative explanations through geometric effects (Chugai 2008) or photon-induced desorption (Soker 2014). The spectra of the last epoch of SN 2017cbv were taken at similar time-scales as the examples above, but show no comparable variations.

## 5. DISCUSSION

The observations suggest that the detected absorption lines stem from gas at interstellar distances. In Ca II H&K, the gas clouds span a velocity range of  $> 170 \text{ km s}^{-1}$ , a dispersion that would be unusual for the disc of a spiral galaxy at the projected distance of 11.6 kpc from the core. Thus some of the gas clouds might be located in the halo of NGC 5643. In the Milky Way, it has been found that the ratio  $N_{\text{Ca II}}/N_{\text{Na I}}$  is lower in gas clouds in the disc than in the halo (Cohen & Meloy 1975). This relation has been used to distinguish between disc and halo absorbing systems in quasar spectra (e.g. Baldwin et al. 1985). In SN 2017cbv, feature VIII has the lowest  $N_{\text{Ca II}}/N_{\text{Na I}}$  value, consistent with gas from the disc. Features IV–VI have higher ratios, suggesting that they could be located in the halo.

Assuming similar ISM properties to our Milky Way, we can infer reddening from  $W_{\text{Na I D}}$  (Poznanski et al. 2012). This suggests a negligible  $E(B - V) = 0.016 \pm 0.003 \text{ mag}$ , in agreement with Hosseinzadeh et al. (2017a).

Some SNe Ia have unusually steep extinction curves (e.g. Amanullah et al. 2015), which could be explained by the presence of CS dust (Goobar 2008). To affect the extinction curve, the dust must be situated at distances closer than a few  $10^{17} \text{ cm}$ . Assuming the dust is traced by Na I and Ca II gas, our observations exclude CS dust at distances of  $\sim 10^{15} - 10^{19} \text{ cm}$  from SN 2017cbv. Hoang (2017) propose that the steep extinction curves are the result of dust grains shattered by radiation pressure. In line with the suggestions in Soker (2014), this could account for the frequently observed blueshifted and unusually deep Na I D profiles (Sternberg et al. 2011; Maguire et al. 2013; Phillips et al. 2013).

Hosseinzadeh et al. (2017a) propose that the early blue excess of SN 2017cbv could be due to the supernova ejecta hitting a non-degenerate companion star (Kasen 2010). The progenitor system containing a sub-giant companion star must have sustained strong stellar winds during accretion. Models suggest that the outflows should excavate large low-density cavities with radii of  $\sim 10^{19} - 10^{20} \text{ cm}$  (Badenes et al. 2007) into the ISM. Since our observations exclude photoionisation of Na I up to  $\sim 2 \times 10^{19} \text{ cm}$  from SN 2017cbv, a cavity larger than this is compatible with Badenes et al. (2007). However, the smaller cavities with a few  $10^{17} \text{ cm}$  predicted for DD He+C/O progenitors (Shen et al. 2013) can be excluded.

## 6. CONCLUSIONS

We have detected multiple Na I and Ca II gas clouds along the LOS to SN 2017cbv, a SN Ia on the outskirts of its host galaxy NGC 5643. We have obtained multi-

epoch high-resolution spectra with UVES starting at an early epoch of  $-14.8$  days before maximum brightness. Due to the extensive time coverage of SN 2017cbv, we are sensitive to photoionisation occurring in gas clouds over a large part of the CS environment. We did not find any time-evolution in any of the detected narrow absorption features, which implies that no detectable Na I gas clouds could be present with  $\sim 8 \times 10^{16} - 2 \times 10^{19} \text{ cm}$  and Ca II within  $\sim 10^{15} - 10^{17} \text{ cm}$  from the explosion. The detected gas clouds must therefore be located further from SN 2017cbv than the outer limit, while any gas closer to the explosion than the inner limit would have been ionised before the first spectrum was obtained.

Hosseinzadeh et al. (2017a) suggest that an early blue excess in the lightcurve could be due to ejecta hitting a non-degenerate companion star in a SD progenitor system. However, they do point out that a lack of a corresponding UV bump is in disagreement with the models of Kasen (2010) and propose several explanations for the discrepancy. A SD progenitor is predicted to have excavated large cavities with radii of  $\sim 10^{19} - 10^{20} \text{ cm}$  into the surrounding ISM and deposit matter at the edges (Badenes et al. 2007). Our observations thus exclude the presence of significant amounts of matter from parts of this range. At the same time, no significant amounts of gas could have been at radii of a few  $10^{17} \text{ cm}$ , distances at which DD He+C/O progenitor models predict matter to be deposited (Shen et al. 2013). There are thus several possible interpretations for our observations, or combinations of them:

- There is no CS gas and the detected absorption features are part of the ISM of NGC 5643 and unrelated to SN 2017cbv.
- There is a CS cavity within the exclusion range, but the Na I and Ca II columns present at the edges are below the detection threshold with  $\log_{10}\{N_{\text{Na I}}^{\text{upper}} [\text{cm}^{-2}]\} = 10.4$  and  $\log_{10}\{N_{\text{Ca II}}^{\text{upper}} [\text{cm}^{-2}]\} = 10.7$ . Assuming normal abundances, the swept up H I mass must be  $M_{\text{H I}}^{\text{CSM}} < 3 \times 10^{-4} \times (R/10^{17} [\text{cm}])^2 M_{\odot}$ , suggesting that the ISM had a very low density.
- The outflowing matter of an SD progenitor system created a cavity larger than  $2 \times 10^{19} \text{ cm}$  (consistent with models of Badenes et al. 2007) and at least some of the detected absorption features correspond to gas deposited at the edges.

Our observations should add useful information to the open progenitor question of SN 2017cbv and SNe Ia in general. A SD progenitor system as that proposed by Hosseinzadeh et al. (2017a) should have a CS environ-

ment comparable to that described in [Badenes et al. \(2007\)](#). While we cannot exclude the full range of possible CS gas shells in this model, we also do not find any evidence for significant amounts of CS gas. This suggests a progenitor model with little to no CS matter for SN 2017cbv. Late time observations, when SN 2017cbv reaches a nebular phase should provide further evidence,

if there was a non-degenerate companion in the progenitor system. In the cases of SNe 2011fe and 2014J, nebular spectra provided strong evidence for the absence of a non-degenerate companion star ([Lundqvist et al. 2015](#)).

The authors acknowledge support from the Swedish Research Council (Vetenskapsrådet) and the Swedish National Space Board.

## REFERENCES

- Amanullah, R., Johansson, J., Goobar, A., et al. 2015, *MNRAS*, 453, 3300
- Badenes, C., Hughes, J. P., Bravo, E., & Langer, N. 2007, *ApJ*, 662, 472
- Baldwin, J. A., Phillips, M. M., & Carswell, R. F. 1985, *MNRAS*, 216, 41P
- Borkowski, K. J., Blondin, J. M., & Reynolds, S. P. 2009, *ApJL*, 699, L64
- Bulla, M., Goobar, A., Amanullah, R., Feindt, U., & Ferretti, R. 2018, *MNRAS*, 473, 1918
- Chomiuk, L., Soderberg, A. M., Chevalier, R. A., et al. 2016, *ApJ*, 821, 119
- Chugai, N. N. 2008, *Astronomy Letters*, 34, 389
- Cohen, J. G., & Meloy, D. A. 1975, *ApJ*, 198, 545
- Dekker, H., D’Odorico, S., Kaufer, A., Delabre, B., & Kotzlowski, H. 2000, in *Society of Photo-Optical Instrumentation Engineers (SPIE) Conference Series*, Vol. 4008, *Optical and IR Telescope Instrumentation and Detectors*, ed. M. Iye & A. F. Moorwood, 534
- Dilday, B., Howell, D. A., Cenko, S. B., et al. 2012, *Science*, 337, 942
- Dong, S., Katz, B., Kushnir, D., & Prieto, J. L. 2015, *MNRAS*, 454, L61
- Ferretti, R., Amanullah, R., Goobar, A., et al. 2016, *A&A*, 592, A40
- Goobar, A. 2008, *ApJL*, 686, L103
- Goobar, A., & Leibundgut, B. 2011, *Annual Review of Nuclear and Particle Science*, 61, 251
- Graham, M. L., Valenti, S., Fulton, B. J., et al. 2015, *ApJ*, 801, 136
- Hoang, T. 2017, *ApJ*, 836, 13
- Hosseinzadeh, G., Sand, D. J., Valenti, S., et al. 2017a, *ApJL*, 845, L11
- Hosseinzadeh, G., Howell, D. A., Sand, D., et al. 2017b, *The Astronomer’s Telegram*, No. 10164, 164
- Huebner, W. F., & Mukherjee, J. 2015, *Planet. Space Sci.*, 106, 11
- Iben, Jr., I., & Tutukov, A. V. 1984, *ApJS*, 54, 335
- Johansson, J., Amanullah, R., & Goobar, A. 2013, *MNRAS*, 431, L43
- Johansson, J., Goobar, A., Kasliwal, M. M., et al. 2017, *MNRAS*, 466, 3442
- Kasen, D. 2010, *ApJ*, 708, 1025
- Kausch, W., Noll, S., Smette, A., et al. 2015, *A&A*, 576, A78
- Koribalski, B. S., Staveley-Smith, L., Kilborn, V. A., et al. 2004, *AJ*, 128, 16
- Kundu, E., Lundqvist, P., Pérez-Torres, M. A., Herrero-Illana, R., & Alberdi, A. 2017, *ApJ*, 842, 17
- Lundqvist, P., Nyholm, A., Taddia, F., et al. 2015, *A&A*, 577, A39
- Maeda, K., Tajitsu, A., Kawabata, K. S., et al. 2016, *ApJ*, 816, 57
- Maguire, K., Sullivan, M., Patat, F., et al. 2013, *MNRAS*, 436, 222
- Margutti, R., Parrent, J., Kamble, A., et al. 2014, *ApJ*, 790, 52
- Modigliani, A., Goldoni, P., Royer, F., et al. 2010, in *Proc. SPIE*, Vol. 7737, *Observatory Operations: Strategies, Processes, and Systems III*, 773728
- Patat, F., Cox, N. L. J., Parrent, J., & Branch, D. 2010, *A&A*, 514, A78
- Patat, F., Chandra, P., Chevalier, R., et al. 2007, *Science*, 317, 924
- Patat, F., Cordiner, M. A., Cox, N. L. J., et al. 2013, *A&A*, 549, A62
- Phillips, M. M., Simon, J. D., Morrell, N., et al. 2013, *ApJ*, 779, 38
- Poznanski, D., Prochaska, J. X., & Bloom, J. S. 2012, *MNRAS*, 426, 1465
- Raskin, C., & Kasen, D. 2013, *ApJ*, 772, 1
- Schlaflly, E. F., & Finkbeiner, D. P. 2011, *ApJ*, 737, 103
- Shen, K. J., Guillochon, J., & Foley, R. J. 2013, *ApJL*, 770, L35
- Simon, J. D., Gal-Yam, A., Gnat, O., et al. 2009, *ApJ*, 702, 1157
- Smette, A., Sana, H., Noll, S., et al. 2015, *A&A*, 576, A77

- Soker, N. 2014, MNRAS, 444, L73
- Sollerman, J., Cox, N., Mattila, S., et al. 2005, A&A, 429, 559
- Sternberg, A., Gal-Yam, A., Simon, J. D., et al. 2011, Science, 333, 856
- . 2014, MNRAS, 443, 1849
- Tartaglia, L., Sand, D., Wyatt, S., et al. 2017, The Astronomer’s Telegram, No. 10158, 158
- Wakker, B. P., & Mathis, J. S. 2000, ApJL, 544, L107
- Webbink, R. F. 1984, ApJ, 277, 355
- Whelan, J., & Iben, Jr., I. 1973, ApJ, 186, 1007